Transport and Communications Science Journal, Vol. 77, Issue 7 (09/2026), 885-898

Transport and Communications Science Journal

A PRELIMINARY ANALYTICAL SCREENING FRAMEWORK FOR UNDER-SLAB RESILIENT MATS IN URBAN RAILWAY SLAB TRACKS

Nguyen Thi Tuyet Trinh*, **Pham Van Ky**

University of Transport and Communications, No. 3 Cau Giay Street, Hanoi, Vietnam

ARTICLE INFO

TYPE: Research Article
Received: 02/07/2026
Revised: 25/08/2026
Accepted: 07/09/2026
Published online: 15/09/2026
https://doi.org/10.47869/tcsj.77.7.1

* *Corresponding author*
Email: tuyettrinh@utc.edu.vn

Abstract. Under-slab resilient mats, referred to here as slab track mats (STMs), can reduce the dynamic force transmitted beneath a concrete track slab. This paper presents a preliminary analytical screening framework that distinguishes dynamic from static stiffness through $\alpha = k_d/k_s$ and equivalent participating mass from total statically supported mass through $\beta = M/m_e$. A harmonically forced single-degree-of-freedom model gives closed-form relationships among a prescribed force-isolation onset frequency, admissible dynamic stiffness and static compression. The illustrative input set is tied to an idealized concrete slab segment and a controlled stiffness-and-damping sensitivity sweep rather than to product-specific properties. For m_e = 5,000 kg, dynamic stiffnesses of 5-40 MN/m give natural frequencies of 5.03-14.24 Hz and force-isolation onset frequencies of 7.12-20.13 Hz. The results show that reducing mat stiffness does not necessarily improve performance because force isolation above the threshold may be accompanied by amplification near resonance. The calculated force transmissibility T is the transmitted-to-applied force ratio at the idealized mat-support interface; $T < 1$ identifies only the force-isolation region of this interface model and is neither insertion loss nor evidence of compliance at a receiving location. The framework provides an early consistency check for defining material-test targets and parameters for subsequent vehicle-track-structure analysis.

Keywords: slab track, under-slab resilient mat, analytical screening framework, vibration isolation, force transmissibility, dynamic stiffness, static stiffness, urban railway.

1. INTRODUCTION

Urban railways often pass through densely developed areas where vibration-sensitive buildings such as homes, offices and hospitals may be located close to the alignment. Wheel-rail excitation is transmitted through the rails, fastenings, track slab, tunnel or viaduct and the surrounding ground, and may be perceived in nearby buildings as vibration or reradiated noise [1-4]. Because slab track is relatively stiff and has limited inherent damping, a resilient layer is often considered to reduce the dynamic force entering the supporting structure.

A slab track mat (STM) is a continuous resilient layer installed beneath a concrete track slab. Its behaviour cannot be described by a single stiffness value: static stiffness, dynamic stiffness, loss factor and fatigue resistance may depend on preload, strain amplitude, frequency, temperature and loading history [5-9]. The stiffness used in analysis should therefore correspond to the expected operating condition, not only to a catalogue value.

Detailed prediction of vibration in the track, ground or receiving buildings requires models of the train, track, supporting structure, soil and receiver, usually supported by laboratory or field data [4, 10- 14]. Such data are often incomplete when STM alternatives are first compared. A simple analytical model can still be useful at this stage, provided that force transmissibility is treated only as an interface force ratio, not as insertion loss or building vibration.

The natural-frequency and force-transmissibility equations used below are established SDOF relations [15, 16]. The methodological contribution is the explicit retention of $\alpha = k_d/k_s$ and $\beta = M/m_e$ throughout a screening sequence that connects a target force-isolation onset frequency to both a dynamic-stiffness limit and the corresponding static compression.

Vietnam-specific context is provided by the Line 3A preparatory survey [17], the national vibration regulation [18], and domestic studies. Nguyen Quang Dung [19] investigated metro-induced ground vibration numerically and examined mitigation measures. Le et al. [20] constructed a coupled train-rail-bridge finite-element model for the Cat Linh-Ha Dong urban railway and updated it by comparison with field measurements. These sources address project conditions, receiver-based assessment and detailed propagation or structural response; the present framework supplies a complementary closed-form screening step.

Against this background, the framework links a prescribed force-isolation onset frequency to admissible dynamic stiffness and static deflection while keeping dynamic and static stiffnesses, and modal and statically supported masses, distinct. It provides a transparent pre-screening step for project specifications, material-test planning and detailed coupled analysis. For Vietnam, the same sequence can support domestic calculation, testing and manufacturing capability for urban railway STMs.

2. SLAB TRACK WITH AN UNDER-SLAB RESILIENT MAT AND ANALYTICAL MODEL

2.1. Structural arrangement and force transmission path

Without an STM, the concrete slab transfers load directly to the supporting structure. Adding the mat introduces a compliant layer, changing both the natural frequency and the dynamic force transmitted across the interface. The mat does not provide isolation at every frequency. Its performance depends on the frequency ratio, damping, preload and the variation of material properties with frequency. Figure 1 shows the idealized force paths and does not represent a particular commercial system.

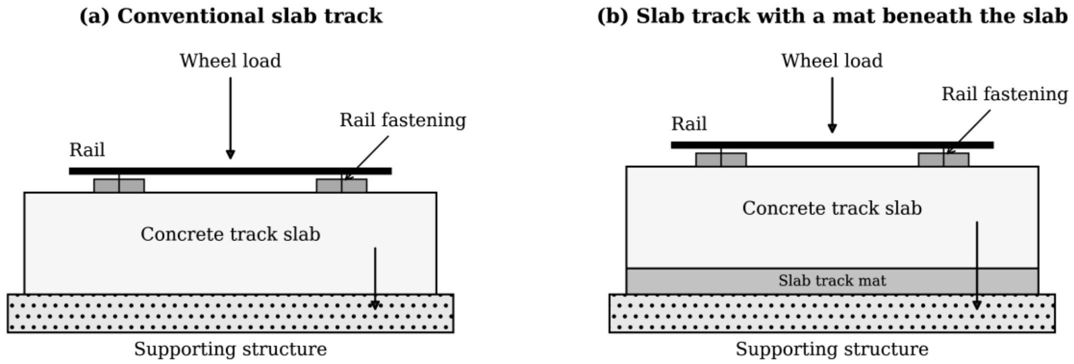

Figure 1. Idealized force paths for (a) conventional slab track and (b) slab track with an under-slab resilient mat.

2.2. Single degree of freedom model

The slab segment and mat are represented by the mass, spring and damper system shown in Figure 2. The support is assumed fixed, the mat is taken as linear within the selected strain range and the applied force is harmonic. In each calculation, the equivalent dynamic stiffness is treated as constant at the selected preload and frequency. Slab bending, rail vibration, wheel-rail interaction and wave propagation through the tunnel and surrounding ground are outside the model.

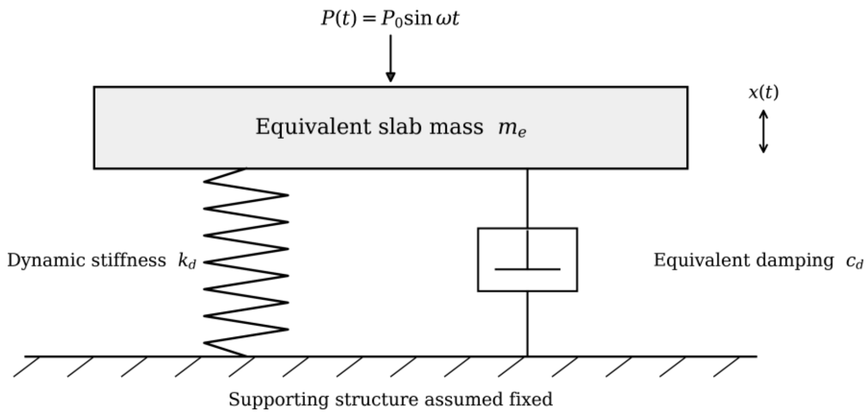

Figure 2. Single-degree-of-freedom representation of a concrete track slab supported by a resilient mat.

The equation of motion of the harmonically forced linear SDOF system is [15, 16]:

$$m_e \ddot{x}(t) + c_d \dot{x}(t) + k_d x(t) = P_0 \sin(\omega t) \quad (1)$$

where m_e is the equivalent participating mass (kg), c_d is the equivalent viscous damping coefficient (N·s/m), k_d is the equivalent dynamic stiffness of the STM beneath the idealized slab segment at the selected preload and frequency (N/m), $x(t)$ is the vertical displacement (m), P_0 is the excitation force amplitude (N), and ω is the excitation circular frequency (rad/s). Let φ be a selected mode shape and j the reference vertical coordinate at the slab-mat interface. If the generalized coordinate is scaled so that $x_j = \varphi_j q$, equality of kinetic energy gives the modal equivalent mass referred to that coordinate as $m_e = \varphi^T M\varphi/\varphi_j^2$. In the rigid vertical-translation idealization used below, m_e reduces to the mass represented by the slab segment. It is therefore determined from the structural idealization and mode shape, independently of axle load. The static stiffness k_s and total statically supported mass M are introduced separately in Section 4.3.

3. METHOD AND PARAMETRIC CASES

3.1. Governing quantities

The undamped natural frequency is calculated as [15, 16]:

$$f_n = \frac{1}{2\pi}\sqrt{\frac{k_d}{m_e}} \tag{2}$$

where f_n is the undamped natural frequency (Hz). The damping ratio and frequency ratio are defined as:

$$\zeta = \frac{c_d}{2\sqrt{k_d m_e}}, r = \frac{f}{f_n} \tag{3}$$

where ζ is the damping ratio (dimensionless), r is the frequency ratio (dimensionless), and f is the excitation frequency (Hz). The force transmitted to the supporting structure contains contributions from both the spring and the damper. For a harmonic force applied directly to the mass, the ratio of transmitted force amplitude to excitation force amplitude is [16]:

$$T = \frac{\sqrt{1+(2\zeta r)^2}}{\sqrt{(1-r^2)^2+(2\zeta r)^2}} \tag{4}$$

T is the dimensionless force transmissibility. Values greater than one indicate amplification, T = 1 defines the boundary, and values below one identify the force-isolation region of the idealized model. From Eq. (4), isolation begins when $r > \sqrt{2}$; therefore:

$$f_{att} = \sqrt{2} f_n \tag{5}$$

where f_{att} (Hz) denotes the force-isolation onset frequency. Equation (5) follows from the viscously damped linear model when k_d is taken as constant in each calculation. Real elastomeric mats are commonly characterized by complex stiffness and a measured loss factor η or tan δ. If the viscous damper is recast as an equivalent complex stiffness at a selected excitation frequency, its equivalent loss factor is $\eta_{eq}(\omega) = \omega c_d/k_d = 2\zeta r$. Thus $\eta_{eq} = 2\zeta$ only at $r = 1$. This relation must not be interpreted as a frequency-independent conversion between a measured material loss factor and the viscous damping ratio. The calculations in Table 2 and Figures 3-4 use ζ directly; no constant loss factor is imposed [6, 13, 16].

3.2. Basis for parameter selection

For dimensional screening, the equivalent participating mass and supported area are tied to an idealized 3.0 m-long, 2.5 m-wide and 0.27 m-thick concrete slab segment with a density of 2,500 kg/m³. Its supported area is A = 7.5 m² and its geometric mass is 5,062.5 kg, rounded to m_e = 5,000 kg for the parametric calculations. This idealized unit establishes a transparent dimensional reference for m_e and A. In project application, m_e is obtained from the relevant mode shape and structural idealization, while the total supported mass M follows from the actual tributary area and loading arrangement.

The frequency scale for the stiffness sweep is anchored to Kuo et al. [11], who reported that the floating-slab track they studied became effective above approximately 10 Hz. This published value is used only as an external frequency-scale reference. If 10 Hz is mapped to the idealized force-isolation onset in Eq. (5), $f_n \approx 10/\sqrt{2} = 7.07$ Hz. For $m_e = 5{,}000$ kg, Eq. (2) then gives $k_d \approx 9.87$ MN/m, rounded to 10 MN/m. The remaining cases are generated by successive halving and doubling (5, 20 and 40 MN/m), producing a controlled logarithmic sensitivity sweep. Their derived f_n and f_{att} values lie below and above the 10 Hz reference and expose the trade-off between isolation onset and static compression. This mapping does not imply equivalence between the published floating-slab system response and the present interface-force metric; it provides an order-of-magnitude anchor for the illustrative sweep. The four stiffnesses are analytical cases rather than catalogue product properties.

The frequencies 5, 10, 20, 30 and 50 Hz in Table 2 sample the response below, near and above the resonances generated by the stiffness sweep. For $A = 7.5$ m², $C_{dyn} = k_d/A$ ranges from 0.00067 to 0.00533 N/mm³. This quantity is an area-averaged bedding modulus for the rigid, uniformly supported segment; local values near rail seats can differ because the pressure distribution is non-uniform. The converted values should therefore be interpreted as model-level area averages; project design uses locally representative stiffness values obtained for the actual contact and product conditions. The lowest stiffness is retained as a sensitivity boundary, and the static compression check determines its admissibility. Candidate mats are then screened for thickness, preload, allowable compression, static and dynamic stiffness, creep, ageing and fatigue [5, 8, 9].

A damping ratio of $\zeta = 0.10$ defines the main analytical cases, while $\zeta = 0.05$ and 0.20 define a broad sensitivity envelope. These damping ratios are analytical sensitivity parameters rather than measured properties of a particular STM. Table 1 also gives the static deflection $\delta_{s,0}$ for the special case $M = m_e$ and $k_s = k_d$; the general relation is derived in Section 4.3. Project calculations replace these reference parameters with stiffness and damping values characterized at the applicable preload, frequency, strain amplitude and temperature.

The numerical results in Tables 1-3 and Figures 3-4 are direct evaluations of Eqs. (2)-(9) for the defined analytical cases. Published measurements enter the discussion only as cited frequency-scale and material-sensitivity benchmarks.

Table 1. Illustrative analytical parameters and derived screening quantities.

k_d (MN/m)	$C_{dyn} = k_d/A$ (N/mm³)	f_n (Hz)	f_{att} (Hz)	$\delta_{s,0}$ (mm)
5	0.00067	5.03	7.12	9.81
10	0.00133	7.12	10.07	4.90
20	0.00267	10.07	14.24	2.45
40	0.00533	14.24	20.13	1.23

4. RESULTS AND DISCUSSION

4.1. Effect of dynamic stiffness on force transmissibility

Equation (2) shows that the natural frequency varies with the square root of dynamic stiffness. As k_d increases from 5 to 40 MN/m, f_n rises from 5.03 to 14.24 Hz and the force-isolation onset frequency rises from 7.12 to 20.13 Hz. Figure 3 and Table 2 therefore show not only a shift of the resonance region, but also the risk of selecting a mat stiffness without reference to the excitation spectrum.

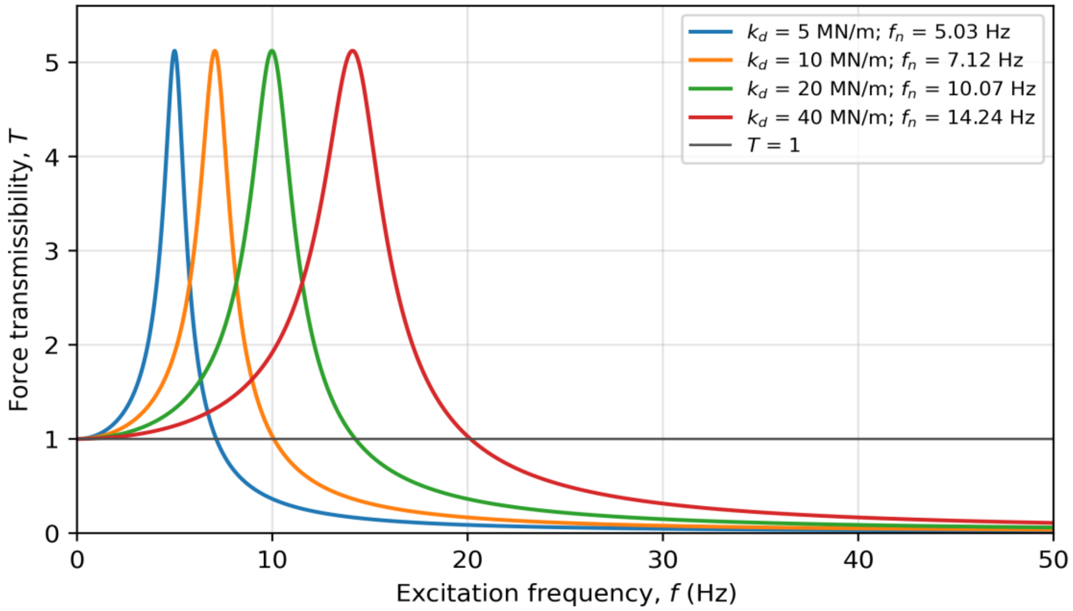

Figure 3. Force transmissibility for four values of equivalent dynamic stiffness (m_e = 5,000 kg; ζ = 0.10).

Table 2. Force transmissibility at representative frequencies for ζ = 0.10 (k_d in MN/m).

f (Hz)	T (k_d = 5 MN/m)	T (k_d = 10 MN/m)	T (k_d = 20 MN/m)	T (k_d = 40 MN/m)
5	5.120	1.921	1.323	1.140
10	0.362	1.025	5.120	1.921
20	0.086	0.166	0.362	1.025
30	0.045	0.078	0.147	0.313
50	0.023	0.036	0.059	0.108

For example, at 5 Hz the 5 MN/m case is close to resonance and *T* is about 5.12, whereas at 10 Hz the 20 MN/m case gives the largest *T*. At 20 Hz, the 5-20 MN/m cases are already in the force-isolation region, while the 40 MN/m case remains near the *T* = 1 boundary. Reducing mat stiffness is therefore not automatically beneficial; the result depends on whether important excitation components lie above or near the isolation threshold and on the dynamic behaviour of the supporting tunnel or viaduct.

4.2. Effect of damping ratio on force transmissibility

Figure 4 illustrates the role of damping. Increasing ζ from 0.05 to 0.20 reduces T at r = 1 from 10.05 to 2.69, confirming that damping is effective mainly near resonance. The values are evaluated at the undamped natural frequency and need not coincide with the exact damped peaks, but the trend is clear.

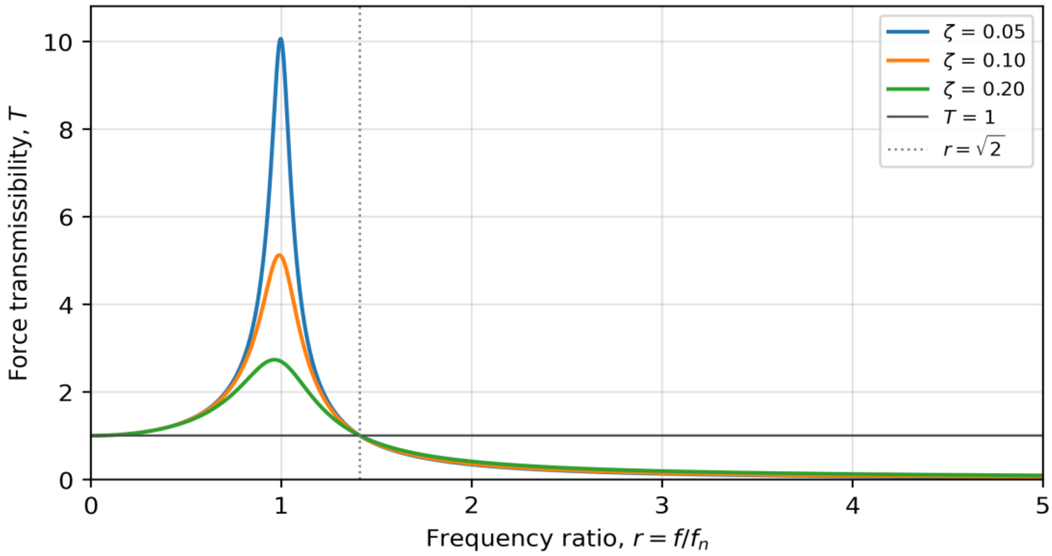

Figure 4. Influence of damping ratio on force transmissibility; the vertical dashed line indicates the theoretical onset of force isolation.

All curves cross T = 1 at r = √2, so damping does not change the isolation threshold in this model. At large r, T approaches 2ζ/r; higher damping can therefore give a slightly larger transmitted force in the high-frequency isolation region. Damping is useful, but it cannot compensate for an unsuitable natural frequency.

As a numerical check, a constant loss factor η = 0.20 was compared with constant viscous damping ζ = 0.10. For the constant-loss-factor representation, $T_\eta = \sqrt{(1 + \eta^2)}/\sqrt{[(1 - r^2)^2 + \eta^2]}$. Relative to the viscous result, the differences in T are 1.1% at $r = 0.5$, 0% at $r = 1$ and $r = \sqrt{2}$, 4.7% at $r = 2$, and 27.8% at $r = 5$. This confirms that the two representations coincide locally near resonance but can diverge at higher frequency ratios; the damping model and its calibration frequency must therefore be reported explicitly.

4.3. Relationship between force isolation and static compressive deformation

From Eq. (2), the dynamic stiffness required to achieve a target natural frequency is:

$$k_d = 4\pi^2 m_e f_n^2 \tag{6}$$

The units used in Eq. (6) are N/m for stiffness, kg for mass, and Hz for frequency. Dynamic and static stiffness are separated by defining the dimensionless ratio $\alpha = k_d/k_s$. Here, k_s is the static stiffness (N/m). A second dimensionless ratio, $\beta = M/m_e$, relates the total supported mass M (kg) to the equivalent participating mass m_e (kg). The static deflection is $\delta_s = Mg/k_s$, where δ_s is expressed in metres. Combining this expression with Eq. (6) gives:

$$\delta_S = \frac{\alpha\beta g}{4\pi^2 f_n^2} \tag{7}$$

where g = 9.81 m/s². The equivalent participating mass cancels from Eq. (7), but the static deflection still depends on α and β. For α = β = 1 and f_n = 5, 7, 10 and 14 Hz, δ_s is 9.94, 5.07, 2.49 and 1.27 mm, respectively. These values differ slightly from Table 1 because that table uses the exact natural frequencies calculated from the selected k_d values. In design, α is obtained from static and dynamic material characterization under representative operating conditions, whereas β follows from the statically supported mass and the participating mass of the selected structural idealization.

Lowering the natural frequency extends the isolation region towards lower frequencies but increases the corresponding static deflection for fixed stiffness and mass ratios. That deflection cannot be inferred from k_d alone because k_s may be markedly different. For example, k_d = 5 MN/m gives an idealized deflection of 9.81 mm when α = β = 1, but this result says nothing about feasibility until the mat thickness, allowable strain, creep and fatigue resistance are known. The static and dynamic checks must therefore be carried out together.

4.4. Interpretation of the stiffness and mass ratios

The product αβ is the multiplicative correction to the baseline α = β = 1. If αβ > 1, the static deflection exceeds the baseline value; if αβ < 1, it is lower. Published STM tests quantify the sensitivity of α. For three polyurethane STM specimens tested at a preload of 0.04 N/mm² and a particle-velocity amplitude of 7 mm/s, Table 3 of Kraśkiewicz et al. [21] reports dynamic-to-static stiffness ratios of 1.63-2.34 at 5 Hz, 2.29-2.97 at 10 Hz and 3.40-4.31 at 20 Hz. Using the overall reported extremes 1.63 and 4.31 as a broad sensitivity envelope, an isolation-onset target f_L = 10 Hz with β = 1 changes the normalized 4.97 mm deflection to 8.10-21.42 mm. The bounding ratios come from different specimens and frequencies; in project application, α should be obtained from material tests under the relevant operating conditions, whereas β is determined from the static tributary mass and the participating mass of the selected structural idealization. Both are therefore project-specific quantities.

The relationships express the main design trade-off. Reducing k_d lowers the force-isolation onset frequency, but it usually increases static deflection. Increasing k_d limits static deflection, but it may place an important excitation component closer to resonance. Damping reduces the resonance peak, but it does not remove the need to select an appropriate natural frequency. A candidate mat is acceptable only when its dynamic stiffness satisfies the isolation requirement and its static stiffness, thickness and long-term behaviour satisfy the deformation limits.

4.5. Model limitations and scope of interpretation

The proposed framework is based on a harmonically forced single-degree-of-freedom system. The slab is represented as rigid, the support as fixed, damping as linear and viscous, and dynamic stiffness as constant within each case. The conversion $C_{dyn} = k_d/A$ is an area average for the uniformly supported segment and does not resolve local pressure concentrations near rail seats. The idealization omits base excitation, distributed wheel loads, slab bending, rail and fastening flexibility, wheel-rail interaction, frequency-dependent complex stiffness and wave propagation through the tunnel, viaduct and ground. Hui and Ng [10], for example, showed that floating-slab bending resonances can influence vibration isolation, illustrating why these effects belong in detailed system analysis.

Accordingly, T is the transmitted-to-applied force ratio at the idealized mat-support interface. Insertion loss and receiver vibration are evaluated separately with a source-path-receiver model and the applicable field assessment procedure. Compliance with QCVN 27:2025/BNNMT or another receiver-based criterion is therefore checked at the affected location. The present relationships supply the preliminary stiffness and compression screen within that broader workflow.

4.6. Internal consistency and external frequency-scale comparison

The calculations were independently recomputed from the closed-form relations. Each curve in Figure 3 crosses $T = 1$ at $f = \sqrt{2}\, f_n$; Table 1 matches Eqs. (2) and (5), and Table 2 matches Eq. (4) to the reported precision. The additional screening calculations presented in Section 5.2 were also independently checked against their governing relations. These checks establish the mathematical and numerical consistency of the screening results.

As an external frequency-scale comparison, Kuo et al. [11] reported that the floating-slab track they studied became effective above approximately 10 Hz. In the present illustrative case, k_d = 10 MN/m and m_e = 5,000 kg give f_{att} = 10.07 Hz. Because the published floating-slab response and the present interface-force transmissibility are different performance measures, the similarity is interpreted strictly as an external order-of-magnitude frequency benchmark for the reference case.

Table 3 further positions the screening framework relative to Refs. [6], [8] and [13]. Those studies contribute material characterization, fatigue evidence or detailed system simulation, whereas the present work contributes a closed-form upstream consistency check.

Table 3. Methodological positioning of the present screening framework against Refs. [6], [8] and [13].

Study	Evidence and model	Main output	Position relative to this study
Zhao et al. [6]	Tests of three STMs; preload- and frequency-dependent material model; coupled vehicle-floating-slab model.	Insertion-loss sensitivity to stiffness representation and axle load.	Provides characterized material input and coupled analysis following preliminary screening.
Huang et al. [8]	Fatigue-loading tests on a polyurethane-mat floating-slab specimen.	Evolution of stiffness and vibration characteristics under cyclic loading.	Supports fatigue and durability qualification of a candidate system.
Xu et al. [13]	Viscoelastic mat models validated against a laboratory slab-track test and used in a track-tunnel-ground model.	Material-model accuracy and detailed system vibration prediction.	Provides frequency-dependent modelling and system prediction after mat characterization.
Present study	Closed-form harmonically forced SDOF screening with explicit α and β.	Admissible dynamic stiffness and static deflection for a target force-isolation onset.	Checks stiffness and compression consistency before product qualification and coupled analysis.

5. IMPLICATIONS FOR URBAN RAILWAYS IN VIETNAM

5.1. Project conditions and assessment criteria

The preparatory survey for Ho Chi Minh City Urban Railway Line 3A, Phase 1, provides an application context. It reports operational design maximum speeds of 80 km/h for the underground section and 120 km/h for the elevated section, 60 kg/m main-line rail, a design axle load of 14 t or 16 t, and slab track or direct-fastened track for the main line [17]. These parameters describe the route and loading context; the analytical frequency sweep is defined independently in Section 3.2.

Train speed converts a spatial irregularity wavelength λ (m) into an excitation frequency f (Hz) through $f = v/\lambda$, where v is expressed in m/s. Axle spacing introduces passage frequencies, while wheel flats and polygonal wear generate impact components; rail fastenings and the slab then modify these inputs before they reach the STM. Reviews identify wheel condition, unsprung mass, speed, track form and transmission characteristics as interacting factors [12]. The 5, 10, 20, 30 and 50 Hz values used in Section 3.2 are analytical sampling frequencies around the calculated resonances. Project selection replaces these sampling points with the relevant project-specific excitation spectrum together with the response of the supporting structure.

Underground and elevated sections require different structural models. In a tunnel, force transmitted through the mat continues through the track base, tunnel lining, surrounding soil and building foundations. On a viaduct, girder bending, local deck response, pier and bearing modes and structural radiation can alter both amplitude and frequency content. Current prediction methods therefore treat the source, transmission path and receiver separately and use transfer functions appropriate to each structural form [14]. The fixed base model used here is suitable only for initial comparison of candidate stiffness ranges.

QCVN 27:2025/BNNMT, issued with Circular 01/2025/TT-BNNMT and effective from 14 November 2025, specifies allowable vibration levels at affected locations, including vibration generated by transport sources [18]. It applies to investment projects that submit applications for appraisal of environmental impact assessment reports, environmental permits or environmental registration after the effective date. Facilities and projects covered by the transitional provisions in Article 3 of the Circular may continue to apply QCVN 27:2010/BTNMT through 31 December 2026; from 1 January 2027, they must meet QCVN 27:2025/BNNMT [18]. The condition $T < 1$ is therefore not a compliance criterion. Compliance must be assessed at receiving locations using a source-path-receiver model and field measurements under the regulations applicable to the project.

5.2. Preliminary stiffness-screening relationships

The 5-40 MN/m cases form the controlled stiffness sweep defined in Section 3.2, with natural frequencies of 5.03-14.24 Hz and force-isolation onset frequencies of 7.12-20.13 Hz. Project application first establishes the lowest required force-isolation frequency from the excitation spectrum and supporting-structure response. The following relationships convert that target into an admissible dynamic-stiffness limit and normalized static deflection; measured k_d, k_s, α and β then define the candidate-specific compression check.

When the project defines the lowest frequency at which force isolation should begin, denoted f_L (Hz), the upper limit of equivalent dynamic stiffness follows from $f_L \geq \sqrt{2}\, f_n$:

$$k_{d,max} = 2\pi^2 m_e f_L^2 \tag{8}$$

where $k_{d,max}$ is the maximum equivalent dynamic stiffness (N/m) at the selected preload and frequency. Combining Eq. (8) with Eq. (7), the static deflection at the isolation threshold, $\delta_{s,b}$ (m), is:

$$\delta_{s,b} = \frac{\alpha\beta g}{2\pi^2 f_L^2} \tag{9}$$

For m_e = 5,000 kg and αβ = 1, an isolation onset at 10 Hz gives $k_{d,max}$ = 9.87 MN/m and $\delta_{s,b}$ = 4.97 mm. An onset at 20 Hz gives 39.48 MN/m and 1.24 mm, respectively. When αβ differs from one, the deflection values should be multiplied by αβ. If k_d changes appreciably with frequency, the calculation should be repeated until the stiffness used in Eq. (2) is consistent with the natural frequency obtained [6].

Table 4 shows how the screening result changes with the lowest required isolation frequency f_L. The final column is written as $\delta_{s,b}/(\alpha\beta)$, so that it can be adjusted using the stiffness and mass ratios of a particular project.

Table 4. Screening relationships for different force-isolation onset frequencies (m_e = 5,000 kg; A = 7.5 m²).

f_L (Hz)	k_d,max (MN/m)	C_{dyn},max (N/mm³)	$\delta_{s,b}/(\alpha\beta)$ (mm)
8	6.32	0.00084	7.77
10	9.87	0.00132	4.97
12.5	15.42	0.00206	3.18
15	22.21	0.00296	2.21
20	39.48	0.00526	1.24

5.3. Project application, testing and verification pathway

For Vietnamese urban railway projects, application proceeds through three linked stages. Stage 1 establishes excitation and transmission characteristics separately for underground and elevated sections from rail roughness, wheel condition, axle-passage effects and supporting-structure response. These inputs identify the frequency bands of concern and the transfer characteristics of each structural form. Comparable operating conditions are used for before-and-after measurements so that insertion loss is evaluated directly.

Stage 2 characterizes candidate mats over the preload, strain amplitude, temperature and frequency range expected in service. The test programme covers static force-deformation behaviour, dynamic or complex stiffness, loss factor, creep, temperature effects, ageing and deterioration under repeated loading. Specimen load is derived from tributary area and load distribution through the slab. EN 17682:2022 provides the test framework for resilient elements in floating slab systems [5], while published results document frequency and loading-history dependence [6, 8, 9, 13].

Stage 3 introduces the characterized material properties into a coupled model of the vehicle, rail, fastenings, slab, mat and tunnel or viaduct, followed by receiver-level assessment. Within this broader project pathway, Figure 5 summarizes the analytical screening sequence: (1) define the target force-isolation onset frequency f_L from the project excitation and transmission characteristics; (2) set the required natural frequency $f_n \leq f_L/\sqrt{2}$; (3) calculate the dynamic-stiffness limit $k_{d,max}$ from Eq. (8); (4) obtain project and test data for k_s, M, mat thickness and damping or loss factor; (5) compute $\alpha = k_d/k_s$ and $\beta = M/m_e$; (6) estimate static compression; (7) check isolation, deformation, creep, fatigue, ageing and durability limits; and (8) pass acceptable candidates to detailed coupled analysis and field verification. Receiver-level compliance is then evaluated using the detailed source-path-receiver model and commissioning measurements under comparable operating conditions.

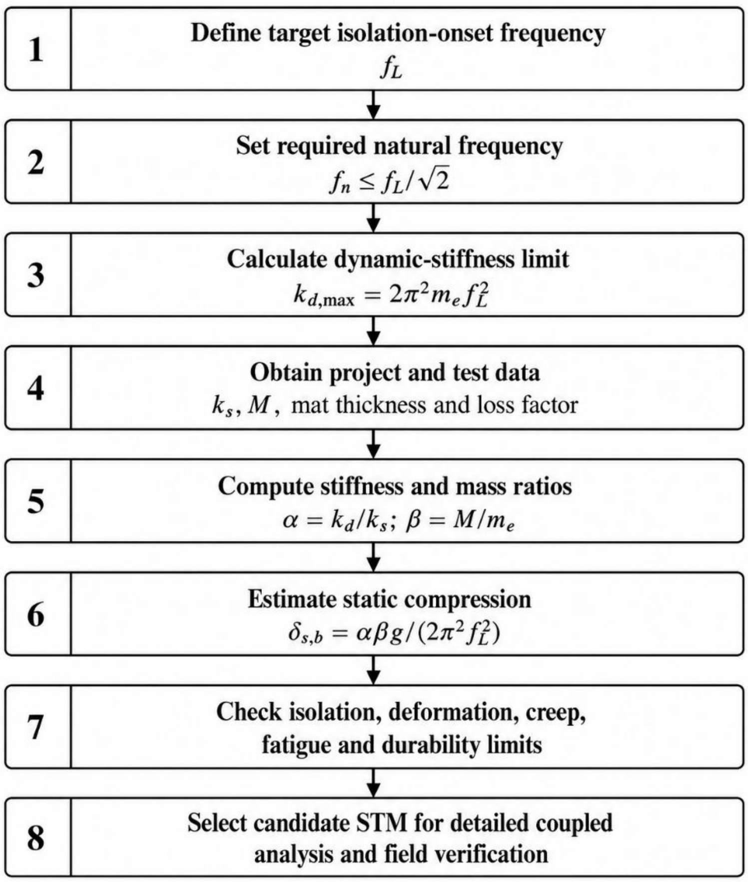

Figure 5. Proposed analytical framework for preliminary screening of under-slab resilient mats.

5.4. Domestic design capability and a pathway to local manufacture

A project specification should define the static and dynamic properties; the preload, frequency, temperature and strain amplitude at which they are measured; the allowable compression; creep and fatigue limits; and the verification method. Catalogue values are useful only when the test conditions are representative of the project.

For Vietnam, priority should be given to domestic capability in calculation, laboratory testing, acceptance criteria and field verification. Imported mats can serve as benchmarks, but design assumptions and acceptance limits should remain under domestic technical control so that products from different suppliers can be compared on a common basis.

Local manufacture follows a staged programme: define target properties, produce laboratory specimens, calibrate material models, test prototype panels, install a trial section and monitor long-term performance. Formulation, manufacturing quality and durability govern whether elastomeric or recycled materials meet the required performance [9]. The relationships developed here supply the initial stiffness and static-deflection targets for that qualification sequence.

6. CONCLUSION

(1) For m_e = 5,000 kg, increasing k_d from 5 to 40 MN/m raises f_n from 5.03 to 14.24 Hz and the force-isolation onset frequency from 7.12 to 20.13 Hz. Stiffer mats reduce static deflection but shift the isolation threshold upwards; stiffness alone is therefore not a measure of isolation performance.

(2) The 5, 10, 20, 30 and 50 Hz values are analytical sampling frequencies around the calculated resonances. The same STM may isolate one frequency range while amplifying another when an excitation component lies near resonance; project screening therefore uses the relevant excitation spectrum.

(3) Increasing damping reduces the resonance peak but does not change the theoretical force-isolation boundary $r = \sqrt{2}$. Damping controls resonance; it does not replace the need to select an appropriate natural frequency.

(4) The ratios $\alpha = k_d/k_s$ and $\beta = M/m_e$ link dynamic isolation and static compression without equating the two stiffnesses or the two masses. For f_L = 10 Hz and β = 1, the sensitivity bounds α = 1.63 and 4.31 from Ref. [21] change the calculated deflection from 4.97 mm to 8.10-21.42 mm, demonstrating the direct influence of the dynamic-to-static stiffness ratio on screening.

(5) For urban railway slab tracks in Vietnam, the framework can support early specification of STM test targets and procurement criteria for underground and elevated sections. Catalogue values, whether for imported or locally manufactured products, should be verified under representative preload, frequency, strain amplitude, temperature and long-term loading conditions.

(6) The framework provides a transparent analytical basis for preliminary STM screening. The 10.07 Hz force-isolation onset for the illustrative 10 MN/m case is of the same order as the approximately 10 Hz effectiveness scale reported by Kuo et al. [11], providing an external order-of-magnitude frequency benchmark for the illustrative screening case. Interface force transmissibility remains the screening metric at the idealized mat-support interface, while receiver-level assessment follows the source-path-receiver procedure.

REFERENCES

[1]. International Organization for Standardization, ISO 14837-1:2005, Mechanical vibration - Ground-borne noise and vibration arising from rail systems - Part 1: General guidance, ISO, Geneva, 2005.

[2]. A. Quagliata, M. A. Shumway, E. Boeker, C. Roof, L. Meister, H. L. Singleton, Transit Noise and Vibration Impact Assessment Manual, FTA Report No. 0123, Federal Transit Administration, Washington, DC, September 2018. https://doi.org/10.21949/1503619

[3]. D. J. Thompson, Railway Noise and Vibration: Mechanisms, Modelling and Means of Control, second ed., Elsevier, 2024.

[4]. W. Zhai, Vehicle-Track Coupled Dynamics: Theory and Applications, Springer Singapore, 2020. https://doi.org/10.1007/978-981-32-9283-3

[5]. European Committee for Standardization, EN 17682:2022, Railway applications - Infrastructure - Resilient element for floating slab system, CEN, Brussels, 2022.

[6]. Z. Zhao, K. Wei, W. Ding, F. Cheng, P. Wang, Evaluation method of the vibration reduction effect considering the real load- and frequency-dependent stiffness of slab-track mats, Materials, 14 (2021) 452. https://doi.org/10.3390/ma14020452

[7]. C. Kraśkiewicz, C. Lipko, M. Płudowska, W. Oleksiewicz, A. Zbiciak, Static and dynamic characteristics of resilient mats for vibration isolation of railway tracks, Procedia Engineering, 153 (2016) 317-324. https://doi.org/10.1016/j.proeng.2016.08.122

[8]. X. Huang, Z. Zeng, Z. Li, X. Luo, H. Yin, W. Wang, Experimental study on vibration characteristics of the floating slab with under-slab polyurethane mats considering fatigue loading effect, Engineering Structures, 276 (2023) 115322. https://doi.org/10.1016/j.engstruct.2022.115322

[9]. C. Kraśkiewicz, P. Majnert, A. Al Sabouni-Zawadzka, P. Mossakowski, M. Zarzycki, Experimental evaluation of under slab mats (USMs) made from end-of-life tires for ballastless tram track applications, Materials, 17 (2024) 5388. https://doi.org/10.3390/ma17215388

[10]. C. K. Hui, C. F. Ng, The effects of floating slab bending resonances on the vibration isolation of rail viaduct, Applied Acoustics, 70 (2009) 830-844. https://doi.org/10.1016/j.apacoust.2008.09.018

[11]. C. M. Kuo, C. H. Huang, Y. Y. Chen, Vibration characteristics of floating slab track, Journal of Sound and Vibration, 317 (2008) 1017-1034. https://doi.org/10.1016/j.jsv.2008.03.051

[12]. S. Ouakka, O. Verlinden, G. Kouroussis, Railway ground vibration and mitigation measures: benchmarking of best practices, Railway Engineering Science, 30 (2022) 1-22. https://doi.org/10.1007/s40534-021-00264-9

[13]. Z. Xu, X. Sun, C. Qiao, T. Wang, M. Ma, Study on modelling method of resilient mat used under floating slab track, Materials, 16 (2023) 3078. https://doi.org/10.3390/ma16083078

[14]. P. Reumers, G. Degrande, G. Lombaert, D. J. Thompson, E. Ntotsios, P. Bouvet, B. Nélain, A. Nuber, Integration of a hybrid vibration prediction model for railways into noise mapping software: methodology, assumptions and demonstration, Railway Engineering Science, 33 (2025) 1-26. https://doi.org/10.1007/s40534-024-00346-4

[15]. A. K. Chopra, Dynamics of Structures: Theory and Applications to Earthquake Engineering, fifth ed., Pearson, Hoboken, NJ, 2017.

[16]. S. S. Rao, Mechanical Vibrations in SI Units, sixth ed., Pearson Education Limited, Harlow, 2018.

[17]. Japan International Cooperation Agency, The Preparatory Survey on Ho Chi Minh City Urban Railway Construction Project (Ben Thanh-Mien Tay Terminal (Line 3A Phase 1)), Final Report (Summary), 2018. https://openjicareport.jica.go.jp/pdf/12305074.pdf

[18]. Ministry of Agriculture and Environment of Vietnam, Circular No. 01/2025/TT-BNNMT dated 15 May 2025 promulgating three national technical regulations on ambient environmental quality, including QCVN 27:2025/BNNMT, National Technical Regulation on Vibration, Hanoi, 2025. https://mae.gov.vn/Pages/chitietvanban.aspx?ItemID=567

[19]. Nguyen Quang Dung, Research on ground vibration and mitigation due to metro operation, Doctoral dissertation, Military Technical Academy, Hanoi, 2013. (in Vietnamese).

[20]. Le Van Vu, Nguyen Huu Quyet, Tran Quang Minh, Nguyen Thi Cam Nhung, Creating a coupled train-rail dynamic model based on the experimental dynamic response of rail structures on urban railways, Transport and Communications Science Journal, 74(9) (2023) 1075-1087. https://doi.org/10.47869/tcsj.74.9.5 . (in Vietnamese).

[21]. C. Kraśkiewicz, A. Zbiciak, W. Oleksiewicz, A. Piotrowski, The influence of selected static and dynamic parameters of resilient mats on vibration reduction of railway tracks, MATEC Web of Conferences, 219 (2018) 05002. https://doi.org/10.1051/matecconf/201821905002